Synthesis and Electrical Transport of Single-Crystal NH$_4$V$_3$O$_8$ Nanobelts

L. Q. Mai,[†,‡] C. S. Lao,[†] B. Hu,[‡] J. Zhou,[†] Y. Y. Qi,[‡] W. Chen,[‡] E. D. Gu,[‡] and Z. L. Wang*,[†]

School of Materials Science and Engineering, Georgia Institute of Technology, Atlanta, Georgia 30332-0245,
School of Materials Science and Engineering, Wuhan University of Technology, Wuhan, 430070, China

Received: July 17, 2006; In Final Form: August 15, 2006

Monoclinic NH$_4$V$_3$O$_8$ single-crystalline nanobelts with widths of 80–180 nm, thicknesses of 50–100 nm, and lengths up to tens of micrometers have been synthesized at large scale in an ammonium metavanadate solution by a templates/catalysts-free route. Such nanobelts grow along the direction of [010]. The individual NH$_4$V$_3$O$_8$ nanobelt exhibits nonlinear, symmetric current/voltage (I/V) characteristics, with a conductivity of 0.1–1 S/cm at room temperature and a dielectric constant of ~130. The dominant conduction mechanism is based on small polaron hopping due to ohmic mechanism at low electric field below 249 V/cm due to Schottky emission at medium electric field between 249 and 600 V/cm and due to the Poole–Frenkel emission mechanism at high field above 600 V/cm.

Introduction

The prospect of using nanostructured objects as components in nanotechnology has led researchers to explore the design of a great variety of interesting materials with tailored morphologies.[1–3] Among them, nanobelts of semiconducting oxides are of considerable interest as functional units for mediating the transport of electrons or optical excitations. Nanobelts with a rectangular cross-section and their well-defined faceted surfaces enable the observation of unique optical-confinement, microcavity effects, catalysis, and piezoelectricity.[4,5] In the past few years, Fabry–Perot microcavities,[6] field effect transistors,[7] and ultrasensitive nanosize gas sensors,[8] nanoresonators,[9] and nanocantilevers[10] have been fabricated based on individual nanobelts.

Vanadium oxide and their derived compounds have attracted much attention due to their outstanding structural flexibility combined with chemical and physical properties,[11] and also because of potential applications in areas such as catalysts,[12] high-energy lithium batteries,[13] chemical sensors, and electrical and optical devices.[14,15] Recently, various methods have been developed to synthesize the nanobelt materials of vanadium oxide[16–18] and their derived compounds.[19,20] However, only limited kinds of single-crystal vanadates with 1-D nanostructures are obtained until now, and the synthesis of new-type nanobelts remains challenging. Herein, we report the synthesis, electrical transport measurements, and conduction mechanism study of a novel nanostructure: NH$_4$V$_3$O$_8$ single-crystalline nanobelts. This is likely to be the first report on the electrical transport measurements on individual nanobelts of multiple vanadates and a proposal about their conduction mechanism.

Experimental Section

In a typical synthesis procedure, ammonium metavanadate (1.50 g) was dissolved in distilled water (90 mL) to form a light-yellow clear solution. Hydrochloric acid was added dropwise to the ammonium metavanadate solution until the final pH of the solution was about 1.5 under stirring. A clear-orange solution was formed and then transferred into a 100-mL Teflon-lined autoclave with a stainless steel shell, which was maintained at 180 °C for 36 h and then cooled to room temperature. The final yellow precipitate was collected and washed with distilled water three times to remove other residues and then dried in air at 80 °C for 8 h.

The products were characterized on a Philips X-ray diffractometer (XRD) with graphite-monochromatized Cu Kα radiation ($\lambda = 0.151\ 48$ nm) and a nickel filter. Fourier transform infrared (FTIR) absorption spectrum was recorded using the 60-SXB IR spectrometer with a resolution of 4 cm^{-1}. Scanning electron micrograph (SEM) images of the samples were obtained in a field emission scanning electron microscopy (FES-EM LEO 1530). Transmission electron microscope (TEM) images and selected area electron diffraction (SAED) pictures were recorded on a transmission electron microscope (JEM 4000EX). The fabrication of a single NH$_4$V$_3$O$_8$ nanobelt-based device was carried out by ac electrophoresis.[19]

Results and Discussion

The XRD pattern of the as-synthesized products is shown in Figure 1. It can be indexed to the monoclinic system with the lattice constants $a = 12.343$ Å, $b = 3.592$ Å, $c = 16.41$ Å, $\beta = 93.30°$ (JCPDS no. 51-0376; (NH$_4$)$_2$V$_6$O$_{16}$·1.5H$_2$O may be regarded as NH$_4$V$_3$O$_8$·0.75H$_2$O). No obvious peaks of other phases are detected, indicating that the product is composed mainly of NH$_4$V$_3$O$_8$ compound.

The FTIR spectrum of the as-received products is displayed in Figure 2. The bands at 1000 and 963 cm^{-1} are assigned to V=O stretching of distorted octahedral and distorted square-pyramids, while the bands at 734 and 533 cm^{-1} are attributed to asymmetric and symmetric stretching vibration of V–O–V bonds.[21] Both bonds at 3161 and 1403 cm^{-1} are assigned to the asymmetric stretching vibrations and the symmetric bending

* Corresponding author. E-mail: zhong.wang@mse.gatech.edu.
† School of Materials Science and Engineering, Georgia Institute of Technology.
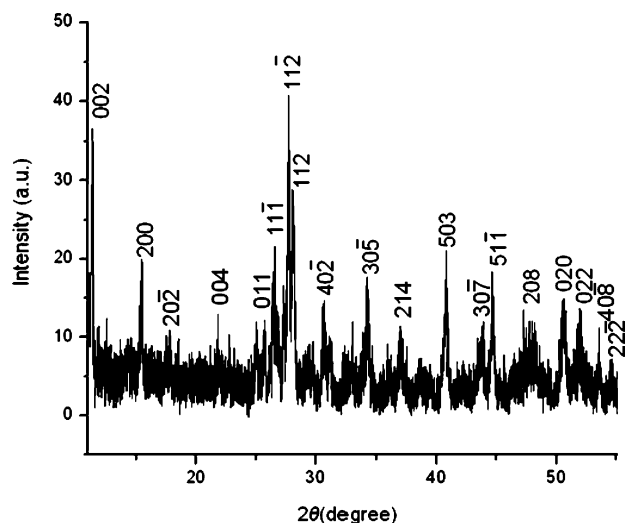‡ School of Materials Science and Engineering, Wuhan University of Technology.

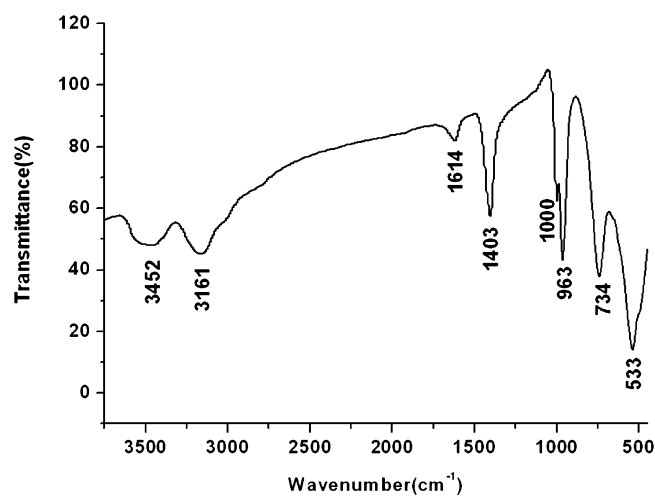**Figure 1.** XRD pattern of the products.

Figure 2. FTIR spectrum of the products.

vibration of NH_4^+.[22] The two bands at 3452 and 1614 cm^{-1} in the spectrum can be assigned to O−H stretching vibrations and H−O−H bending motion, respectively. Thus, the FTIR spectrum further confirms that the nanowires are composed of $NH_4V_3O_8 \cdot 0.75H_2O$.

Parts a−c of Figure 3 show a low-magnification SEM image, EDS spectrum, and a high-magnification SEM image of $NH_4V_3O_8$ single-crystalline nanobelts, respectively, and reveal that the resulting products are composed mainly of beltlike nanostructures with well-defined facets. As shown by the arrowheads, the rectangular ends of the beltlike materials can be seen clearly. The width and thickness of the nanobelts are in the range of 80−180 and 50−100 nm, respectively, with typical lengths up to tens of micrometers. Energy-dispersive X-ray spectroscoy (EDS) further confirms the presence of N, V, and O (H cannot be detected by EDS).

The belt-like shape of $NH_4V_3O_8$ is further characterized by TEM technique (Figure 3d). The selected area electron diffraction (SAED) pattern (Figure 3e) taken from the nanobelt is indexed to monoclinic $NH_4V_3O_8$. Significantly, the diffraction pattern did not change as the electron beam was moved along the nanobelt, indicating that the whole nanobelt is a single crystal, with a preferential growth direction along the [010] direction.

As marked by the circles in Figure 3c and f, approximately 4% of the reaction products exhibit a "bent-belt" morphology. This bending arises from the formation of a twin boundary at
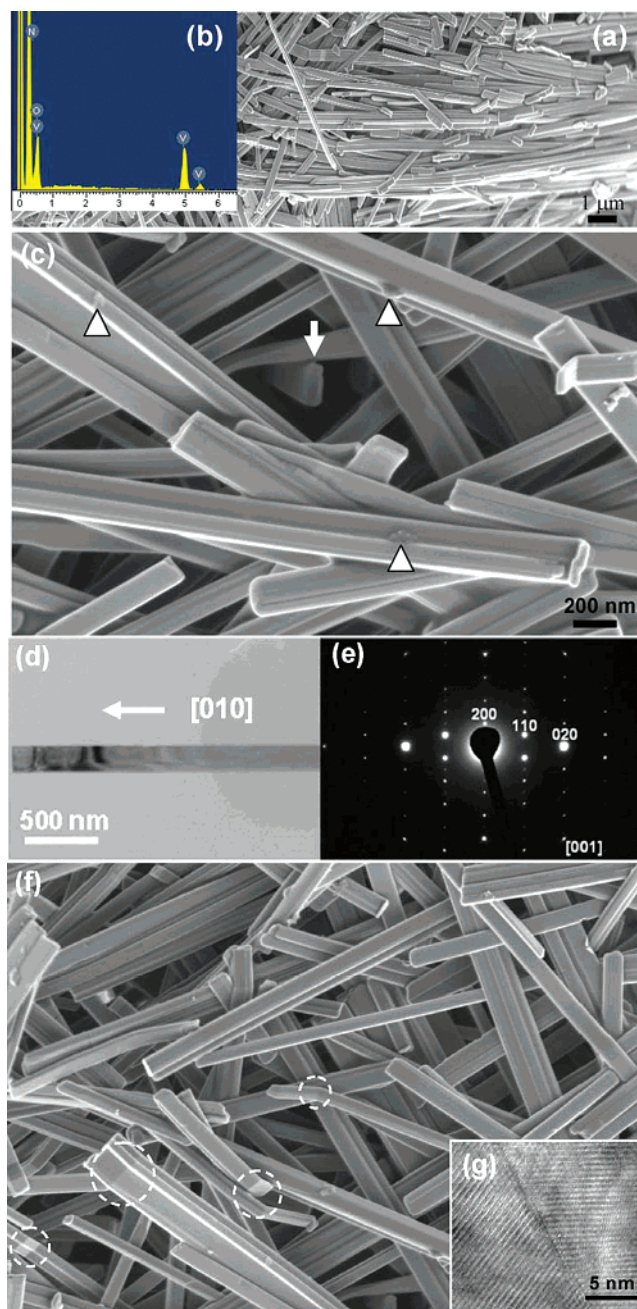

Figure 3. Low-magnification SEM image (a), EDS spectrum (b), and high magnification SEM image (c) of $NH_4V_3O_8$ nanobelts. In (b), the arrowheads indicate the rectangular ends of the nanobelts, the circles mark the bent or twinned nanobelts, and the triangles show some bulk and surface defects. TEM image (d) and the corresponding SAED pattern (e) of a $NH_4V_3O_8$ nanobelt. (f) SEM image of the bent or twinned $NH_4V_3O_8$ nanobelts, which are marked by circle. (g) The representative HRTEM image of the twin boundary present in a nanobelt.

the (100) planes, which causes an abrupt 120° change in direction of the wire. Electron microscope images and diffraction data show that, like the straight belts, each branch of these twinned belts also grows along the [010] direction. The representative high-resolution TEM image of the twin boundary of the nanobelt is shown in Figure 3g.

The SAED pattern in the inset of Figure 3e, combined with the rectangular end shown in Figure 3c, allows the unambiguous determination of the facet surfaces of the $NH_4V_3O_8$ nanobelts. Specifically, the top facet of the nanobelt in Figure 3d, which is perpendicular to the electron beam, is (001). The crystallographic symmetry of monoclinic $NH_4V_3O_8$ then dictates that
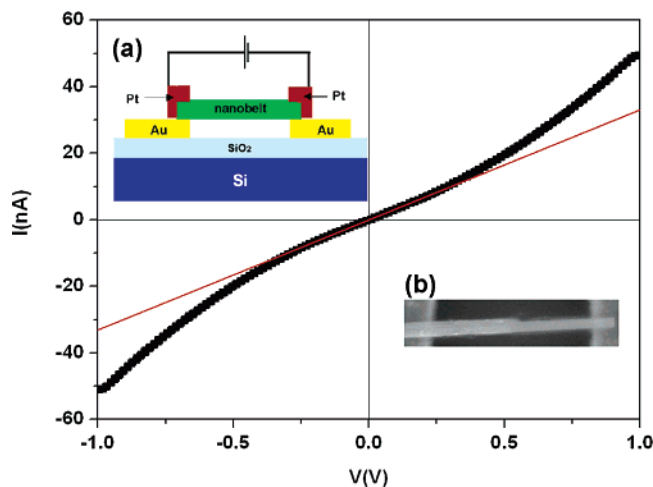
Figure 4. I/V curve of individual nanobelt. Insets: A and B show the schematic view and the SEM image of the individual nanobelt electrode, respectively.

the side facet bounding the same nanobelt should be (100). This conclusion is supported by the SAED patterns of the nanobelts investigated to date. The (001) and (100) facets are crystallographically equivalent, low-index, and therefore, low surface energy. This observation explains the rectangular ends or cross-sections of the $NH_4V_3O_8$ nanobelts as well as their unique growth direction.

The basic reaction we employed for the synthesis of the $NH_4V_3O_8$ nanobelts can be formulated as follows:

$$6NH_4VO_3 + 4H^+ \rightarrow (NH_4)_2V_6O_{16} + 4NH_4^+ + 2H_2O \qquad (1)$$

In this process, ammonium metavanadate in aqueous solution forms NH_4^+ and VO_3^-. As the temperature increases, meta-

vanadate groups start to agglutinate into VO_4 tetrahedra chains, in which the tetrahedra, are connected by sharing corners. When the reaction proceeds to a certain extent, the tetrahedral chains coalesce to form VO_5 pyramid sheets bridged by H_2O between vanadium ions, in which pyramids are connected at corners or edges, and NH_4^+ inserts between VO_5 pyramid sheets, resulting in the formation of $(NH_4)_2V_6O_{16}\cdot1.5H_2O$ nanobelts. Owing to the existence of NH_4^+ between VO_5 pyramid sheets, the nanobelts are expected to have good electrical conductivity so that they may be used as nanosensors.

We have built the contacts using e-beam lithiography for measuring the electrical transport along a single nanobelt. The I/V curve of a single $NH_4V_3O_8$ nanobelt at room temperature is shown in Figure 4. A schematic view and the SEM image of the individual nanobelt electrode are shown in the insets A and B of Figure 4, respectively. With a contact resistance of about 10 MΩ, the effective length and cross-section of the sample is approximately 8×10^{-4} cm and 500×100 nm^2, respectively, so we can deduce the conductivity value of $\sim$0.2 S/cm, and this value can range from 0.1 to 1 S/cm depending on the samples.

Notably, the $NH_4V_3O_8$ nanobelt sample exhibits nonlinear, symmetric current/voltage (I/V) characteristics. To further study the electrical conduction mechanism, we have simulated the I/V curve. It is found that the obtained characteristic is symmetrical and behaves linearly for an electrical field lower than 249 V/cm. This behavior may be explained by the ohmic mechanism of conductivity in the low electrical field (<249 V/cm). A further increase in the applied voltage results in an exponential behavior in the current mechanism. Because the thickness of the nanobelt is more than 50 nm, the tunnel current can be ignored. Figure 5 presents the positive part of the I/V characteristics of the transversal system, rebuilt as a function of log(*I*). The aim of this plot is to analyze the conduction mechanism in higher fields (en-
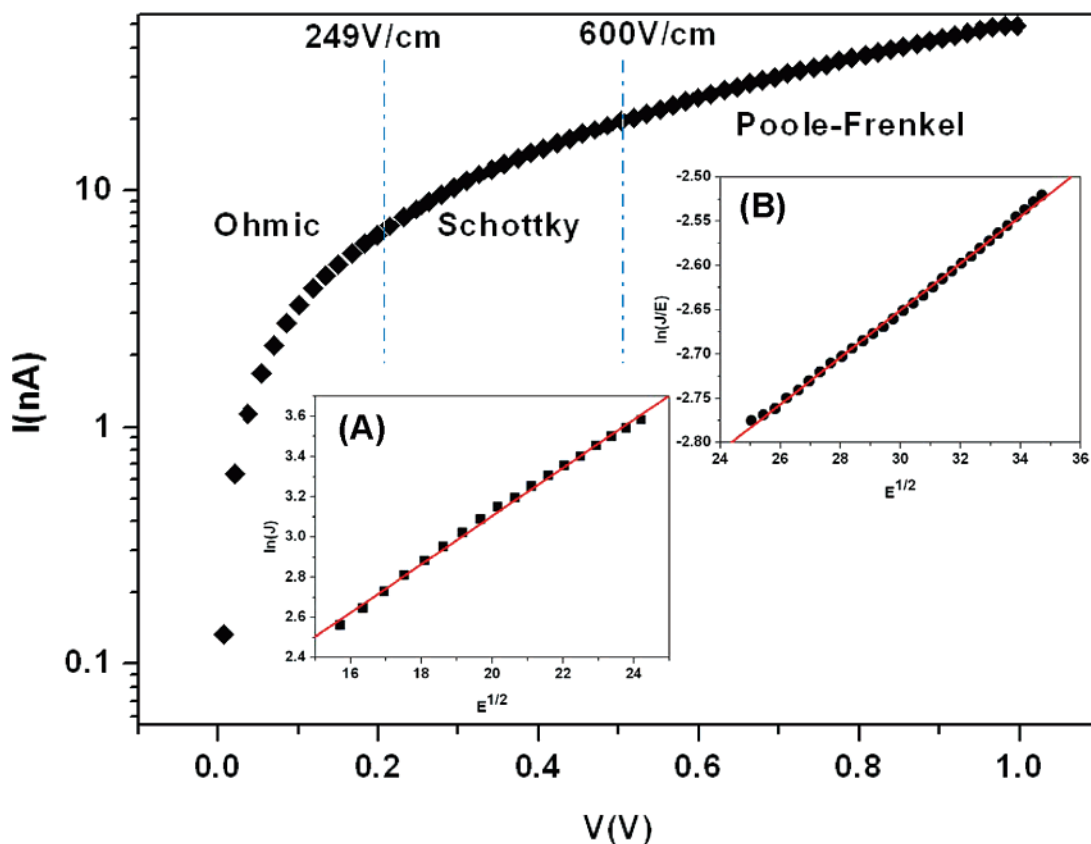

Figure 5. Positive part of the I/V characteristics of the transversal system, rebuilt as a function of log(*I*). Insets: A and B show the experimental plot of ln(*J*) vs $E^{1/2}$ at the electric field between 249 and 600 V/cm, and the experimental plot of ln(*J/E*) vs $E^{1/2}$ at the electric field more than 600 V/cm.

Letters

J. Phys. Chem. B, Vol. 110, No. 37, 2006 **18141**

larged voltages). The logarithm of the current density is plotted against the square root of the electric field [$\ln(J)$ versus $E^{1/2}$], as shown in inset A of Figure 5. The straight-line nature obtained at a medium electric field between 249 and 600 V/cm implies the Schottky emission. The Schottky current density is expressed as follows:[24]

$$\ln J = \frac{\beta_{SE}}{kT}\sqrt{E} + \left[\ln(AT^2) - \frac{q\phi}{kT}\right] \quad (2)$$

where A is a constant, ϕ is the Schottky barrier height, q is the electronic charge, k is Boltzmann's constant, and E is the electric field. The constant β_{SE} is given by

$$\beta_{SE} = \sqrt{\frac{q^3}{4\pi\epsilon_0\epsilon_r}} \quad (3)$$

where ϵ_r is the dielectric constant, ϵ_0 is the permittivity of the free space. The dielectric constant obtained from the slope (ϵ_r = 132.1) is consistent with that obtained from the C−V technique (ϵ_r = 131.6).[24]

Interestingly, with the increase of electrical field, the experimental data fit well to the Poole−Frenkel mechanism. Unlike the Schottky mechanism, defined by thermoelectron emission of the free charge carriers, the Poole−Frenkel transport is defined by emission from structural defects in energetic traps. A straight line (see inset B in Figure 5) is obtained at a high electric field (>600 V/cm) in the experimental plot of $\ln(J/E)$ versus $E^{1/2}$. This suggests that the leakage current is dominated by the P−F conduction mechanism at a relatively high electric field. The expression for the P−F current density is as follows:[23]

$$\ln\left(\frac{J}{E}\right) = \frac{\beta_{PF}}{\xi kT}\sqrt{E} + \left(\ln C - \frac{q\phi}{\xi kT}\right) \quad (4)$$

where $q\phi$ is the ionization potential in eV, which is the amount of energy required for the trapped electron to overcome the influence of the trapping center when no field is applied, $\beta_{PF}\sqrt{E}$ is the amount by which the trap barrier height is reduced by the applied electric field E, C is a proportionality constant, and k is the Boltzmann constant. The coefficient ξ is introduced in eq 4 for taking into account the influence of the trapping or acceptor centers ($1 < \xi < 2$).[23] When $\xi = 1$, the conduction mechanism is termed as the normal P−F effect, whereas it is termed the P−F effect with compensation or the modified P−F effect when $\xi = 2$. In this case, the semiconductor contains a non-negligible number of carrier traps. The P−F constant, β_{PF}, is given by

$$\beta_{PF} = \sqrt{\frac{q^3}{4\pi\epsilon_0\epsilon_r}} \quad (5)$$

where ϵ_0 is the permittivity of the free space, and ϵ_r is the dynamic dielectric constant. The dielectric constant (ϵ_r = 129.3) obtained from the slope of the straight line in the Poole−Frenkel plot also corresponds to that obtained from the C−V technique.[24] The $NH_4V_3O_8$ nanobelts are found to have some bulk and surface defects, as shown by triangles in Figure 3b. Therefore, the Poole−Frenkel emission in this case is the preferable mechanism that agrees with the results described in the reference.[25]

Conclusions

In summary, we have demonstrated a facile environmentally friendly route to synthesize pure $NH_4V_3O_8$ single-crystal nanobelts at a large scale by hydrothermal treatment of aqueous solu-

tions of NH_4VO_3 under acid conditions. Such nanobelts grow along the direction of [010]. The widths, thicknesses, and lengths of the nanobelts are in the range of 80−180 nm, 50−100 nm, and tens of micrometers, respectively. The conductivity of one individual $NH_4V_3O_8$ nanobelt is estimated to be 0.1∼1 S/cm at room temperature with a dielectric constant of ∼130. On the basis of small polaron hopping, the dominant conduction mechanism is due to ohmic mechanism at low electric field below 249 V/cm, due to Schottky emission at medium electric field between 249 and 600 V/cm and due to the Poole−Frenkel emission mechanism at high field above 600 V/cm. It is anticipated that the novel $NH_4V_3O_8$ single-crystalline nanobelts with high conductivity may have unique applications in nanoelectrodes or nanosensors.

References and Notes

(1) Iijima, S. *Nature* **1991**, *354*, 56.
(2) Kresge, C. T.; Leonowicz, M. E.; Roth, W. J.; Vartuli, J. C.; Beck, J. S. *Nature* **1992**, *359*, 710.
(3) Pan, Z. W.; Dai, Z. R.; Wang, Z. L. *Science* **2001**, *291*, 1947.
(4) Huang, M. H.; Mao, S.; Feick, H.; Yan, H. Q.; Wu, Y. Y.; Kind, H.; Weber, E.; Russo, R.; Yang, P. D. *Science* **2001**, *292*, 1897.
(5) Song, J. H.; Wang, X. D.; Riedo, E.; Wang, Z. L. *Nano Lett.* **2005**, *5*, 1954.
(6) Yan, H. Q.; Johnson, J.; Law, M.; He, R. R.; Knutsen, K.; McKinney, J. R.; Pham, J.; Saykally, R.; Yang, P. D. *Adv. Mater.* **2003**, *15*, 1907.
(7) Arnold, M. S.; Avouris, P.; Pan, Z. W.; Wang, Z. L. *J. Phys. Chem. B* **2003**, *107*, 659.
(8) Comini, E.; Faglia, G.; Sberveglieri, G.; Pan, Z. W.; Wang, Z. L. *Appl. Phys. Lett.* **2002**, *81*, 1869.
(9) Bai, X. D.; Gao, P. X.; Wang, Z. L.; Wang, E. G. *Appl. Phys. Lett.* **2003**, *82*, 4806.
(10) Hughes, W. L.; Wang, Z. L. *Appl. Phys. Lett.* **2003**, *82*, 2886.
(11) Chen, W.; Xu, Q.; Hu, Y. S.; Mai, L. Q.; Zhu, Q. Y. *J. Mater. Chem.* **2002**, *12*, 1926.
(12) Prosini, P. P.; Xia, Y. Y.; Fujieda, T.; Vellone, R.; Shikano, M.; Sakai, T. *Electrochim. Acta* **2001**, *46*, 2623.
(13) Mai, L. Q.; Chen, W.; Xu, Q.; Peng, J. F.; Zhu, Q. Y. *Chem. Phys. Lett.* **2003**, *382*, 307.
(14) Liu, P.; Lee, S. H.; Cheong, H. M.; Tracy, C. E.; Pitts, J. R.; Smith, R. D. *J. Electrochem. Soc.* **2002**, *149*, H76.
(15) Muster, J.; Kim, G. T.; Krstic, V.; Park, J. G.; Park, Y. W.; Roth, S.; Burghard, M. *Adv. Mater.* **2000**, *12*, 420.
(16) Liu, J. F.; Li, Q. H.; Wang, T. H.; Yu, D. P.; Li, Y. D. *Angew. Chem., Int. Ed.* **2004**, *43*, 5048.
(17) Liu, J.; Wang, X.; Peng, Q.; Li, Y. *Adv. Mater.* **2005**, *17*, 764.
(18) Yu, J.; Liu, S.; Cheng, B.; Xiong, J.; Yu, Y.; Wang, J. *Mater. Chem. Phys.* **2006**, *95*, 206.
(19) Lao, C. S.; Liu, J.; Gao, P. X.; Zhang, L. Y.; Davidovic, D.; Tummala, R.; Wang, Z. L. *Nano Lett.* **2006**, *6*, 263.
(20) Wu, X. C.; Tao, Y. R.; Dong, L.; Hong, J. M. *J. Mater. Chem.* **2004**, *14*, 901.
(21) Azambre, B.; Hudson, M. J.; Heintz, O. *J. Mater. Chem.* **2003**, *13*, 385.
(22) Dobley, A.; Ngala, K.; Yang, S. F.; Zavalij, P. Y.; Whittingham, M. S. *Chem. Mater.* **2001**, *13*, 4382.
(23) Chiu, F. C.; Wang, J. J.; Lee, J. Y.; Wu, S. C. *J. Appl. Phys.* **1997**, *81*, 6911.
(24) Chakraborty, S.; Bera, M. K.; Dalapati, G. K.; Paramanik, D.; Varma, S.; Bose, P. K.; Bhattacharya, S.; Maiti, C. K. *Semicond. Sci. Technol.* **2006**, *21*, 467.
(25) Golan, G.; Axelevitch, A.; Sigalov, B.; Gorenstein, B. *J. Optoelectron. Adv. Mater.* **2004**, *6*, 189.